5-19-2006

Traveltime Inversion of Vertical Radar Profiles

William P. Clement
Boise State University

Michael D. Knoll
Boise State University

GEOPHYSICS, VOL. 71, NO. 3 (MAY-JUNE 2006); P. K67–K76, 10 FIGS.
10.1190/1.2194527

Traveltime inversion of vertical radar profiles

William P. Clement[1] and Michael D. Knoll[1]

ABSTRACT

Traveltimes of direct arrivals in vertical radar profiles (VRPs) are tomographically inverted to estimate the earth's electromagnetic (EM) velocity between a surface transmitter and a downhole receiver. We determine the 1D interval velocity model that best fits the first-arrival traveltimes by using a weighted, damped, least-squares inversion scheme. We assess the accuracy of the velocity model using synthetic traveltimes from a known velocity-distribution model simulating an unconfined aquifer. The inverted velocity profile closely matched the velocity profile of the input model in the synthetic examples. Using vertical radar profile data from an unconfined aquifer near Boise, Idaho, we inverted traveltimes to obtain velocity estimates at the well location. The velocity change at a depth of 2.0 m corresponds well with the measured depth to the water table of 1.95 m, and at depths between 2 and 18 m, the velocities ranged between 0.06 and 0.1 m/ns. Our estimates approximately match the velocity distribution determined from neutron-derived porosity logs at depths greater than about 2 m. An important function of inverse methods is to assess (quantitatively and qualitatively) the uncertainty of inverted velocity estimates. We note that the velocity values in the upper and lower parts of the inverted model are not as well constrained compared to those between the depths of 4 and 13 m. From the model resolution and model covariance matrices of the real-data inversion, we determine the uncertainty in our velocity model, leading to more reliable interpretations of the subsurface.

INTRODUCTION

Ground-penetrating radar (GPR) is used widely in near-surface investigations. Common-offset reflection profiling is used to determine the structure and stratigraphy in many areas. However, these data are displayed as time sections because depths are poorly constrained. To better convert the time axis to depth, subsurface velocity is estimated between pairs of subsurface reflections in common-midpoint (CMP) or wide-angle-reflection and refraction (WARR) profiles (Davis and Annan, 1989; Tillard and Dubois, 1995). Thus, surface reflection methods usually do not provide highly detailed estimates of the subsurface velocity.

Accurate electromagnetic (EM) velocities are needed for processing routines such as migration. Furthermore, accurate EM velocities can be converted to estimates of important hydrological properties such as porosity (Knoll and Knight, 1994) or soil moisture content (Greaves et al., 1996). Recently, crosshole tomography and zero-offset profiling have been used to characterize the subsurface distribution of velocity values (Peterson et al., 1999; Binley et al., 2001). Tomography provides a detailed 2D velocity model, but estimating model reliability is difficult because of the large number of parameters. Alternatively, zero-offset crosshole profiles (ZOPs) are fast and easy to acquire but may not provide an accurate velocity-depth profile because of bending ray paths.

Another method for obtaining detailed EM velocity estimates is vertical radar profiling (VRP) (Knoll and Clement, 1999). The acquisition geometry of a VRP is similar to the better-known vertical seismic profile (VSP). We extend the VSP concept to VRPs (Knoll and Clement, 1999; Zhou and Sato, 2000). An important goal of VRP surveys is to obtain an accurate model of velocity changes with depth. Unlike Zhou and Sato (2000), who use reflections in the VRP data to provide a stratigraphic image of the subsurface, we use VRPs to determine a detailed velocity model of the subsurface.

Other researchers are using VRPs to investigate the subsurface. Pringle et al. (2003) collected VRP data by conducting surveys down cliff faces. The VRPs extended the depth of imaging from constant-offset GPR surveys acquired at the surface. They also compared velocities from VRPs to velocities from CMPs. Their analysis showed that velocities from VRPs and CMPs were consistent. Cassini et al. (2004) used VRPs to characterize the deep vadose zone. Their inversion technique to determine interval velocities is similar to ours. They included error bounds on velocity estimates but did not provide a rigorous assessment of the model error. Tronicke and Knoll (2005) discussed pitfalls in acquiring

Manuscript received by the Editor October 18, 2001; revised manuscript received December 22, 2004; published online May 19, 2006.
[1]Center for Geophysical Investigation of the Shallow Subsurface, Boise State University, 1910 University Drive, Boise, Idaho 83725. E-mail: billc@cgiss.boisestate.edu; mknoll@cgiss.boisestate.edu.

VRP data. They looked at the influence of critically refracted waves and the radiation patterns of the transmitter and receiver antennae on VRP traveltimes and amplitudes. Analyzing near-offset VRP data lessens the influence of critically refracted waves.

This paper describes in more detail the VRP velocity-estimation method used in Knoll and Clement (1999) and Buursink et al. (2002) and extends the analysis of VRP traveltime inversion presented in those papers. To assess the reliability of the algorithm, we start with a synthetic example. We also explore the model resolution and uncertainty of the inverse solution through appraisal analysis. The analysis then is extended to a field example from an alluvial, unconfined aquifer near Boise, Idaho.

To provide a rigorous estimate of interval velocities, we use a least-squares, linear inversion method to compute the velocity within model layers. We use the inverse of the kernel matrix to assess the reliability and uncertainty of our velocity estimates. Including uncertainty estimates with our model provides a more reliable and useful estimate of the subsurface velocity distribution.

GENERAL INVERSE THEORY

To describe our inversion scheme, we start with a system of equations in the form

$$\mathbf{Ax} = \mathbf{b}, \tag{1}$$

where $\mathbf{x}$ is the vector containing the model parameters, $\mathbf{b}$ is the vector of the observations, and $\mathbf{A}$ is the kernel matrix that relates the model to the data. To solve the matrix equation, we must find the inverse of the matrix $\mathbf{A}$. For our solution, we choose a model that minimizes the difference between the observed and calculated traveltimes, the data residuals, in a least-squares (L_2) sense:

$$E = \|\mathbf{b} - \mathbf{Ax}\|^2. \tag{2}$$

Minimizing the data misfit equation results in the normal equation

$$\mathbf{A^T Ax} = \mathbf{A^T b}. \tag{3}$$

Solving for the model $\mathbf{x}$ yields

$$\mathbf{x} = (\mathbf{A^T A})^{-1}\mathbf{A^T b}. \tag{4}$$

We restrict the number of model parameters to be less than the number of observations, so the system of linear equations is overdetermined. However, because geophysical problems are typically ill-conditioned or ill-posed (Parker, 1994; Snieder and Tampert, 1999), solutions using simple matrix inversion are unsatisfactory. To dampen fluctuations in the solution, we minimize the data residuals and the model norm (Aki and Richards, 1980; Menke, 1989):

$$E = \|\mathbf{W_d}(\mathbf{b} - \mathbf{Ax})\|^2 + \lambda^2\|\mathbf{W_m}(\mathbf{x} - \mathbf{x_0})\|^2, \tag{5}$$

resulting in the weighted, damped, least-squares solution

$$\mathbf{x} = \mathbf{x_0} + (\mathbf{A^T W_d^T W_d A} + \lambda^2\mathbf{W_m^T W_m})^{-1}\mathbf{A^T W_d}(\mathbf{b} - \mathbf{Ax_0}). \tag{6}$$

In this equation, $\mathbf{x_0}$ is the starting model, $\mathbf{W_d}$ is the data-weighting matrix, $\mathbf{W_m}$ is the model-weighting matrix, and λ^2 is the regularization parameter that balances the data and model misfit. We use a reasonable (though crude) guess of the slowness distribution in the subsurface for the starting model. For the data weighting matrix $\mathbf{W_d}$, we use an estimate of the error in the observations. The choice of the least-squares solution dictates that $\mathbf{W_d}$ is the inverse of the variance of the Gaussian distribution of the errors in our data. Constraints on the model are invoked with the choice of $\mathbf{W_m}$. We can choose the identity matrix $\mathbf{I}$ for $\mathbf{W_m}$, or we can choose to regularize the solution with a flatness (first-difference) or smoothness (second-difference) constraint (Menke, 1989). We invoke Occam's Razor to choose the simplest solution using minimum structure (Constable et al., 1987). The goal of interpretation is to glean as much information from the data as possible without misrepresenting the solution detail.

Measures of model reliability

To better understand the reliability of our inverse solution, we compute the generalized inverse $\mathbf{A}^\dagger$ (Menke, 1989):

$$\mathbf{A}^\dagger = (\mathbf{A^T W_d^T W_d A} + \lambda^2\mathbf{x W_m^T W_m x})^{-1}\mathbf{A^T W_d}. \tag{7}$$

From $\mathbf{A}^\dagger$, we calculate the model resolution matrix as

$$\mathbf{R} = \mathbf{A}^\dagger\mathbf{A}, \tag{8}$$

and the model covariance matrix as

$$\mathbf{Cov_m} = \sigma^2\mathbf{A}^\dagger\mathbf{A}^{\dagger\mathbf{T}}, \tag{9}$$

where σ is the standard deviation of the data (Aki and Richards, 1980; Menke, 1989).

The model resolution matrix provides an estimate of the geometrical resolution of the model (Snieder and Trampert, 1999). In other words, the model resolution matrix is a measure of how well each parameter is resolved in the original matrix. If the model resolution matrix is the identity matrix $\mathbf{I}$, then the system is perfectly resolved. In an overdetermined, noise-free system, the model resolution matrix should be the identity matrix. If the model resolution matrix contains off-diagonal elements, then these values indicate that the parameter of interest is an average of the adjacent parameters weighted by the nonzero elements.

The model covariance matrix indicates how repeatable the estimator is under random data variations (van Wijk et al., 2002). Alternatively, the model covariance matrix is a measure of how data error maps into model error. The model covariance matrix contains the model variances along the diagonal and the model covariances in the off-diagonal elements. If model covariance elements are small, small data errors will result in small model errors; if the elements are large, small data errors result in large model errors (Menke, 1989).

Choosing λ^2

Chi-squared (χ^2) is a measure of the goodness-of-fit of the model to the data (Constable et al., 1987) and has the form

$$\chi^2 = \frac{\mathbf{e}^T\mathbf{e}}{\sigma^2}, \tag{10}$$

where **e** is the data-residuals vector and σ is the standard deviation of the error in the observations. We use χ^2 to determine the optimal value of λ^2 through a line search. The line-search routine computes a large number of solutions with different values for λ^2. We choose the λ^2 value that results in a χ^2 between $N \pm \sqrt{2N}$, where N is the number of observations.

VRP INVERSION

Inversion for interval velocity is common for VSPs (Lines et al., 1984; Stewart, 1984; Pujol et al., 1985, 1986; Lizarralde and Swift, 1999); we extend this method to VRPs. The geometry of a VRP experiment is shown in Figure 1a. The data consist of first-arrival traveltimes between the transmitting antenna and the receiver locations (Figure 1b). The inversion procedure consists of determining the travel paths through the model (matrix **A**) and inverting for the model parameters. In the VRP case, the model parameters are slowness (reciprocal of velocity) values.

The forward-modeling equation used to compute traveltimes is

$$t = \int_{\text{ray}} \frac{1}{v(l)} \mathrm{d}l, \tag{11}$$

where t is the traveltime along a given ray, v is the velocity along that ray, and l is the length along the raypath. The raypaths depend on the model parameters resulting in a nonlinear system of equations. We use several steps to linearize the system. First, the inversion solves for slowness instead of velocity, removing velocity from the denominator. Second, a straight ray approximates the true raypath between transmitter and receiver, removing dependence on raypath. If the direction of the raypaths is nearly parallel to the velocity gradient (i.e., approximately vertical), straight rays are a valid assumption. We investigate the validity of the straight-ray assumption with a synthetic model. Finally, the inversion uses horizontal layers of constant velocity and thickness to reduce our solution to layer slownesses instead of both slownesses and thicknesses. This linearization simplifies the inversion procedure significantly. A ray is traced from the transmitter to each receiver. The ray length in each layer for each transmitter-receiver pair is an element of the matrix **A**.

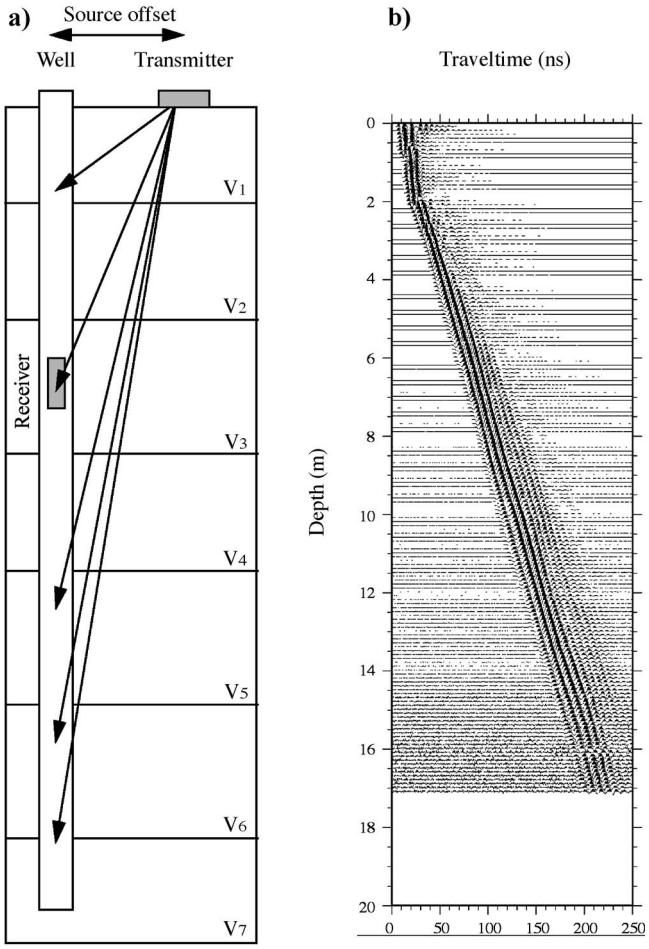

Figure 1. (a) Model showing the geometry of VRP acquisition and (b) data from a VRP in a shallow, alluvial, unconfined aquifer.

Synthetic example

To test our VRP inversion routine, we inverted traveltimes from a synthetic experiment. Figure 2 shows the input velocity model. The synthetic model consists of five constant-velocity layers representing a shallow, unconfined aquifer. The uppermost layer (above the ground surface) represents the air and has a velocity of 0.3 m/ns. Below this layer is a 2-m-thick layer (surface to 2-m depth) representing the vadose zone with a velocity of 0.14 m/ns, a 1-m-thick layer (2 to 3 m) with a velocity of 0.06 m/ns, a 7-m-thick layer (3 to 10 m) with a velocity of 0.09 m/ns, and a 10-m-thick layer (10 to 20 m) with a velocity of 0.06 m/ns. These last three layers represent units in the saturated zone with different porosities and water contents.

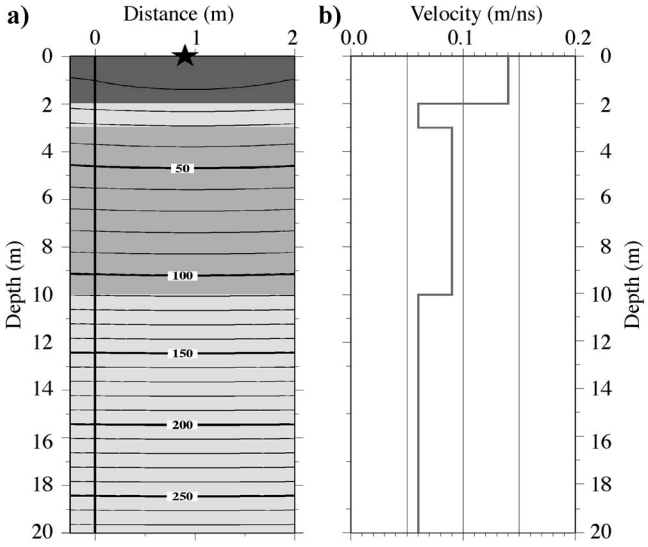

Figure 2. (a) Synthetic velocity model and computed traveltimes simulating a VRP. The source point is 0.9 m from the well. The gray shading corresponds to different EM velocities. (b) The velocity plotted as a 1D function of depth.

The EM velocity in porous media is strongly dependent on fluid content. Air has a dielectric constant of 1 and an EM velocity of 0.3 m/ns, whereas water has a dielectric constant of about 80 and an EM velocity of about 0.03 m/ns. Thus, sediments with air-filled pores have a faster EM velocity than similar sediments with water-filled pores.

The transmitting antenna is offset 0.9 m from the well. There are 201 simulated receiver positions spaced every 0.10 m down the well, starting at 0-m depth. We generate the synthetic traveltimes with a finite-difference approximation to the Eikonal equation (Hole and Zelt, 1995).

Figure 3a shows the results of the inversion. Because we are inverting synthetic, noise-free traveltimes, we placed no constraints on the solution ($\mathbf{W_d} = \mathbf{I}$; $\mathbf{W_m} = \mathbf{I}$; $\lambda^2 = 0$). Using these parameters is equivalent to solving the least-squares problem

$$\mathbf{x} = \mathbf{x_0} + (\mathbf{A}^T\mathbf{A})^{-1}\mathbf{A}^T(\mathbf{b} - \mathbf{A}\mathbf{x_0}). \quad (12)$$

The inversion routine calculates the velocities for eighty 0.25-m-thick layers. The layer thickness limits the resolution of subsurface layering. We selected 0.25 m for the layer thickness because this thickness is close to the dominant wavelength of the data in the slowest unit, but larger than the receiver step size.

Above 2 m, the inverted model is a poor match to the input model. The velocity starts at 0.08 m/ns, gradually increases to about 0.17 m/ns at a depth of 1 m, and then decreases to 0.13 m/ns at a depth of 2 m. The poor fit is because of the straight-ray assumption used to linearize the inversion. At shallow receiver depths (0 to 1.5 m), the first arrivals are refracted at the air/surface boundary (Tronicke and Knoll, 2005). However, the inverse routine assumes that the energy has propagated directly from the source to the receiver along straight raypaths. Thus, the path lengths and velocity values for layers near the surface are not accurate.

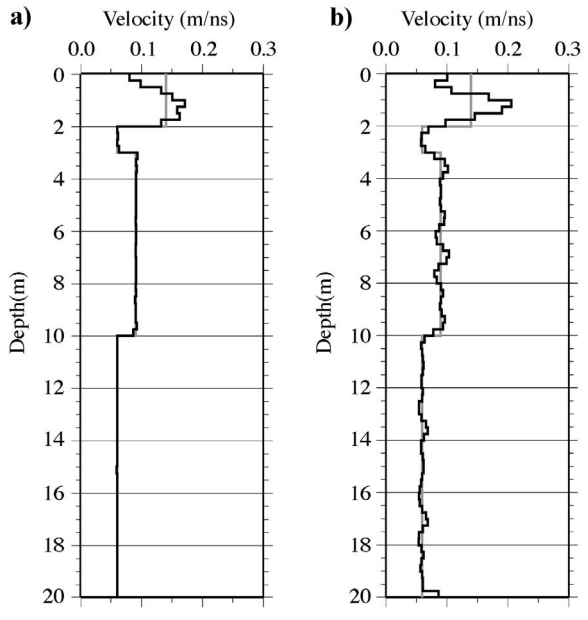

Figure 3. Velocity inversions for the model in Figure 2. (a) Noise-free synthetic traveltimes and (b) noisy synthetic traveltimes. The gray line in both plots is the input velocity model. The source is 0.9 m from the well.

Below 2 m, the inverted model is nearly the same as the input model. Even at the sharp velocity changes at depths of 2, 3, and 10 m, the inverted velocities closely match the true velocities. The close match indicates that the straight-ray assumption is valid below depths of about 2 m and that inverted velocities are a good estimate of the velocity in the subsurface.

When we add noise to the traveltimes, we obtain a worse fit to the input model. To simulate realistic, noisy data, we added random noise with zero mean and a 0.25 ns standard deviation, as well as a percentage (0.5%) of the total traveltime of the ray to the synthetic arrivals. The 0.25 ns standard deviation is about half the sample interval typically used in acquiring 250-MHz VRP data. In earlier work, we determined the picking uncertainty to be between 0.1 ns and 1.2 ns, depending on data quality. Adding a small percentage of the total traveltime of the ray to the synthetic arrivals ensures that the noise increases as the traveltime increases. Adding only the standard deviation to each traveltime causes the earlier, high signal-to-noise arrivals to have more noise as a percentage of their traveltime than the later, low signal-to-noise arrivals. Thus, our synthetic traveltimes have an increase in uncertainty with increasing traveltime, as we have observed with field data.

Using the same inversion parameters as for the noise-free case, results in an unrealistic, wildly oscillating velocity model. To improve the velocity model, we regularized the solution by adding smoothness constraints ($\mathbf{W_m}$ is related to the second difference operator by $[-1,2,-1]^T[-1,2,-1]$) and using a λ^2 of 0.31. The solution oscillates somewhat around the input model (Figure 3b). Again, the shallowest 2 m are poorly modeled, as they are in the noise-free case. The velocity oscillates between 0.079 and 0.10 m/ns between depths of 3 and 10 m, mostly because of the inversion trying to fit the noise. However, the velocity changes at depths of 2, 3, and 10 m are clearly discerned in the inverted model. By comparing the results of our inversion routine to synthetically generated traveltimes, we can better understand the limitations of the inverse method.

A limitation with smooth regularized inversion is that the method seeks a smooth solution. The oscillations near the velocity jumps are artifacts of the smoothness constraint. The input synthetic traveltimes are computed for a model with a distinct velocity jump, but the inversion tries to smooth the sharp velocity boundary, resulting in the velocity oscillations. Although the oscillations are artifacts, the sharp velocity changes at depths of 2 and 3 m are still represented in the inverted velocity model. The change at a depth of 10 m is more difficult to see. The poor match to the input model at this depth is the result of the decrease in the signal-to-noise ratio of the data. The synthetic tests indicate that the inversion scheme can model changes in velocity, but care must be taken to not overinterpret the model.

Error analysis

An advantage of inverse theory is that various statistical estimates of the uncertainty can be computed, such as data residuals, in our velocity model. The noise-free synthetic velocity model fits the data well. To two significant digits after the decimal point, the residuals range between 0.38 and 0.13 ns, with a mean of 0.00 ns, a standard deviation of 0.03 ns, and a root mean square (rms) value of 0.00 ns. The small errors are expected because of the noise-free synthetic traveltimes.

Also, as expected, the noisy synthetic traveltimes have larger traveltime residuals than the noise-free traveltimes. These residu-

als range between −0.53 and 1.04 ns, with an rms value of about 0.02 ns, a mean of 0.07 ns, and a standard deviation of 0.31 ns. Although these statistical values are larger than those for the noise-free simulation, the traveltime residuals indicate that the model adequately predicts the synthetic traveltimes.

Because we have a small, linearized system, we can compute $\mathbf{A}^{\dagger}$ (equation 7) directly, allowing us to determine the model resolution (equation 8) and model covariance (equation 9) matrices for our velocity model. As mentioned, well-resolved features have a model resolution value of 1, such as the noise-free simulation. Features with small variance values are less prone to errors in the data than large variance values. In the more realistic noisy simulation, the diagonal elements of the model resolution matrix are 0.41, except near the top and bottom of the model. The sum of the model resolution values for any single layer is 1. If the diagonal model resolution values are less than 1, nonzero off-diagonal elements occur in the model resolution matrix. The nonzero off-diagonal elements indicate that the velocities are a weighted average of the surrounding velocities. In the noisy simulation, the velocity estimates are primarily dependent on the velocities in the three overlying and underlying layers. Imposing regularization on the solution will force the routine to average over several layers. Thus, regularizing the solution decreases the resolution in the resulting model.

We expect the highest model resolution values to be located near the top of the model where many rays travel through the model layers. Conversely, we expected the smallest model resolution values to be located near the bottom of the model where ray coverage is relatively low. Interestingly, in the synthetic modeling study using realistic noisy data, model resolution values were nearly constant for most of the model parameters. The model resolution value at the shallowest depth is 0.63. Below this depth, the values are about 0.41 to a depth of 19.0 m. At the bottom 0.5 m of the model, model resolution values oscillate between slightly higher and lower values, with the model resolution value at the deepest layer being about 0.30. The increase in model resolution at the base of the model may be a boundary effect due to the lack of deeper layers. The nearly constant model resolution values between depths of 0.5 m and 19.0 m indicate that the velocities are resolved to the same degree throughout the model.

The variance of the model parameters from the noisy simulations is 0.004 ns^2/m^2; the smallest values are at the top, and the largest values are near the bottom of the model. The variance provides an indication of the error bounds on the velocity estimate. The smaller values at the top of the model indicate that these velocities are better constrained. All rays travel through these upper layers, providing more information about these layers. Only a few rays sample the lowest layers; they are less tightly constrained. Except for the lowermost layers, the model velocities are well constrained.

Field example

To demonstrate the traveltime inversion method, we analyzed a VRP data set (profile 18 from July 11, 2000) collected in well A1 at the Boise Hydrogeophysical Research Site (BHRS). The BHRS is a research well field located on a gravel bar of the Boise River where much is known about the subsurface distribution of hydrologic and geophysical properties (Barrash and Knoll, 1998; Knoll and Clement, 1999; Peterson et al., 1999; Tronicke et al., 2004; Tronicke and Knoll, 2005). Wells at the BHRS penetrate about 20 m of coarse, alluvial deposits that have been subdivided into five units with varying amounts of cobble and sand and different porosity geostatistics (Barrash and Clemo, 2002). A red clay, 3 m thick, underlies the aquifer. The water table during the experiment was located at 1.95 m below land surface.

Figure 4 shows the VRP data collected with a Mala RAMAC/GPR system using 250-MHz borehole antennae. Each trace consists of 800 samples that were vertically stacked 256 times in the field. The sample interval is 0.397 ns, and the signal bandwidth is 20 to 200 MHz. The surface transmitting antenna was oriented radially from the wellhead, with the center point of the antenna 0.9 m from the well. The receiving antenna was lowered in well A1, acquiring data at fixed locations every 0.10 m from a depth of 0.05 m to a depth of 18.05 m below land surface. Processing included time zero correction, dc bias removal, and bandpass filtering. We also divided each trace by its rms amplitude to balance the traces for plotting. The data have high signal-to-noise ratios, especially above 12 m.

The most obvious feature in the VRP data is the slope change of the first arrivals at a depth of about 2.0 m. This slope break indicates a change in velocity that corresponds well with the measured level of the water table (1.95 m below land surface) in this well. The decrease in slope also indicates that the apparent velocity decreases in the saturated zone. First arrivals at depths less than about 1.8 m involve energy that has been refracted at the air/ground in-

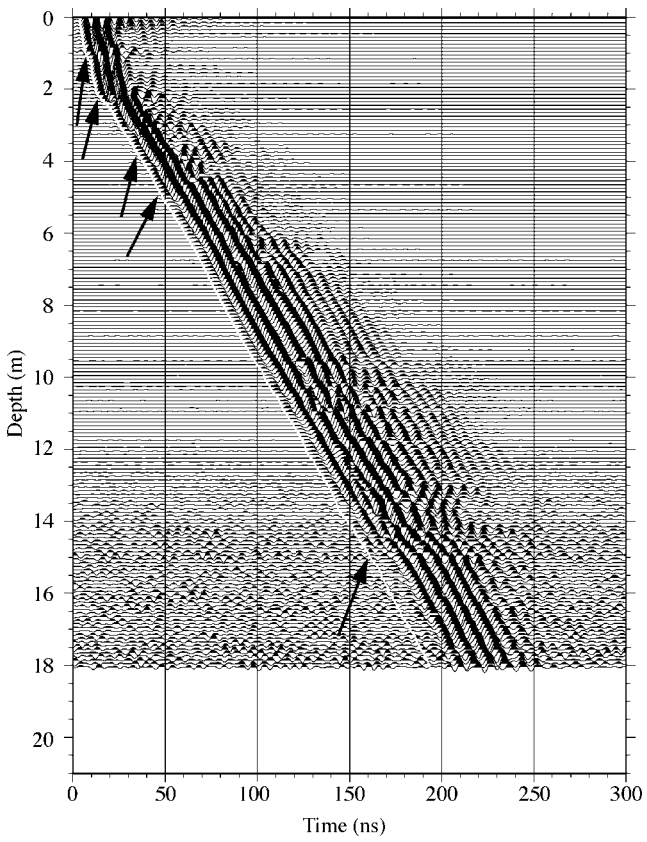

Figure 4. VRP data from well A1 at the BHRS. The source point (feedpoint of the transmitting antenna) was located 0.9 m from the axis of the well. The receiver depths are with respect to the land surface. The solid white line marks the observed first arrival picks used in the inversion. The arrows point to reflections.

terface (Tronicke and Knoll, 2005). Below a depth of about 2.0 m, first arrivals are direct arrivals. The small changes in slope indicate small velocity changes with depth.

Also apparent in the data is upgoing reflection energy. The reflections in Figure 4 are difficult to see because we processed the data to highlight the first arriving energy. Processing to enhance upgoing reflection energy shows many reflections. These reflections, although ringy in character as the first arrivals, suggest that several large impedance contrasts exist at the site. The shallowest reflection identified in Figure 4 is at a depth of about 1.0 m. A stronger reflection is observed at a depth of about 2.0 m, corresponding to the water table. Other strong reflections occur at depths of 4.0, 5.0, and 15.0 m. The presence of upgoing reflections in the VRP indicates changes in electromagnetic impedance at these depths.

We picked 181 first-arrival transmitter-to-receiver traveltimes, corresponding to depths between 0.05 and 18.05 m. To estimate the picking uncertainty in our observations, five other people used the same method to pick similar data from another well. From analysis of their picks, we determined that the standard deviation of the time picks was 0.1 ns. This procedure provides a crude estimate of the error resulting from mispicking the direct arrivals. Other sources of error are present in the data, but we cannot measure their contribution to the data error at this point.

Results

The results of the weighted, damped, least-square inversion (equation 6) are presented in Figures 5–10. We parameterized the model with 0.25-m-thick layers and used a starting model with a slowness equivalent to 0.08 m/ns. The inversion regularized the solution using a smoothing (second difference) matrix. The line search to find λ^2 resulted in a value of 0.143; χ^2 (equation 10) was about 181, the number of observations.

Figure 5 shows the velocity estimates from the 1D inversion. The velocities decrease from an average of around 0.18 m/ns for depths above 2 m to about 0.09 m/ns for layers below this depth. Above a depth of 2 m, velocities fluctuate from about 0.27 m/ns at the surface to 0.12 m/ns at a depth of around 1 m, then increase to 0.27 m/ns at a depth of 1.9 m. The water table causes a sharp velocity decrease at a depth of about 2 m.

Above a depth of 2 m, the high velocities are faster than expected for unsaturated sediments. However, the first arrivals are probably refracted at the air/ground interface (Tronicke and Knoll, 2005), not direct arrivals as assumed in the inversion routine. From the synthetic modeling, velocities above a depth of 2 m were inaccurate because the straight-ray approximation poorly models the true raypath. These factors indicate that the high velocities are not the velocities of the undisturbed, unsaturated sediments, but more likely have been influenced by airwave energy and other interference effects and should be ignored.

Below a depth of 2 m, the velocities fluctuate around 0.09 m/ns. These slower velocities are because of the high water content of the sediments. Small velocity changes, ranging between 0.065 and 0.11 m/ns, occur throughout the saturated zone. Again, these velocities are consistent with the composition and porosity variations of the water-saturated sediments at the site.

A slower velocity of 0.065 m/ns occurs near a depth of 2.5 m. A high-porosity sand lens, determined from well cores, may cause the slow velocity. Alternatively, the inversion may try to overcompensate for the discontinuity at the water table. A small error in traveltime picking may cause the high-velocity layer at a depth of 12 m. The error bars on the velocities indicate that this layer is more poorly constrained than most of the model.

The strong reflections indicated by the arrows in Figure 4 coincide with velocity changes in the model. The reflection at a depth of about 2.0 m coincides with the water table. The reflections at depths of 4.0 and 5.0 m approximately coincide with the top and bottom, respectively, of the thin, high-velocity layer at that depth in the velocity model. The strong reflection at a depth of about 15 m roughly coincides with the transition from low to high velocity in the derived velocity model at that depth. Other reflections are in the VRP, but linking them to specific velocity changes is difficult because of their ringy character and the gradational velocity changes in the model.

These reflections could be used to constrain the traveltime inversion (Moret et al., 2004). We would allow the velocity change across the reflecting boundary to be large instead of varying smoothly. This process imposes an assumed structure on the model parameters. The ringy character of the VRP reflections makes accurate depth determination difficult. We prefer to let the inversion algorithm choose the depths of the velocity changes and use the reflections to corroborate the inverted velocity model.

The VRP velocity model can also be compared to EM velocity estimates derived from a neutron porosity log collected in well A1 (Barrash and Clemo, 2002). We converted the porosity values to

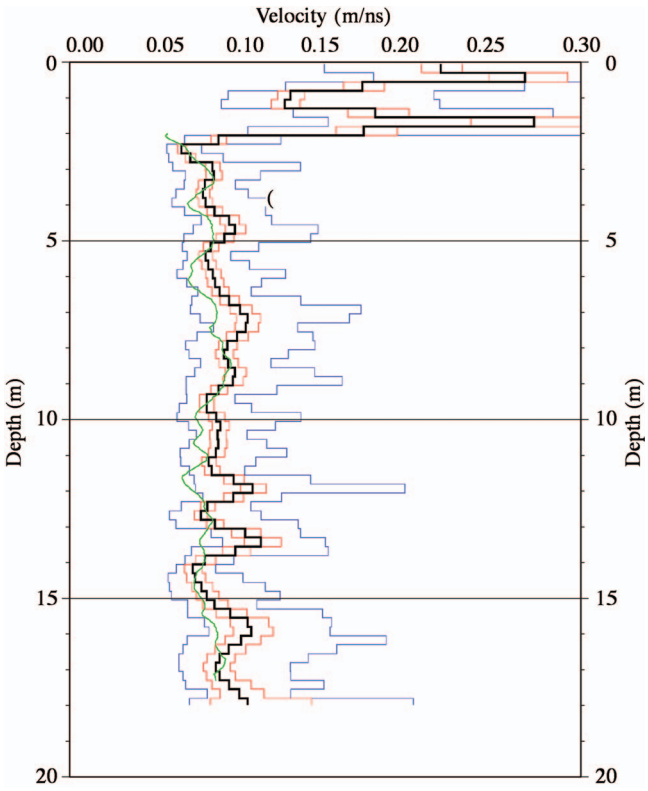

Figure 5. Velocity model from the inversion of A1 VRP traveltime picks. The black line is the velocity model. The thin blue lines are twice the standard deviation computed from the multiple realizations of the slowness model. The thin red lines are twice the standard deviation as determined from the diagonal elements of the covariance matrix. The thick orange line is the velocity derived from the neutron log in well A1.

EM velocities based on the time-propagation model, a volume-weighted average of the refractive indices (square root of the dielectric constant) of water and the matrix material (Wharton et al., 1980; Knoll, 1996). The sediments at the BHRS are cobble-dominated sands and gravels. For the velocity conversion, we used 80 for the dielectric constant of water (k_w) and 4.6 for the dielectric constant of the siliclastic rock matrix (k_m). The velocity formula is:

$$v = \frac{v_{air}}{\sqrt{\phi}\sqrt{k_w} + (1 - \phi)\sqrt{k_m}}, \quad (13)$$

where ϕ is the porosity derived from the neutron log. Figure 5 shows the velocity calculated from the neutron-derived porosity. Porosity-derived velocities are not available above a depth of 2.0 m because the neutron log was not analyzed for porosity values in the vadose zone. For much of the model, the porosity-derived velocities are within the 95% confidence limits of the inverted model. In the shallowest 10 m, the inversion velocities and the derived velocities follow similar trends and are about the same magnitude. Near a depth of 12 m, the porosity-derived velocity decreases, whereas the VRP-derived velocity increases. The oscillatory nature of the inverted model may cause the dissimilar velocity at a depth of 12 m. Overall, the strong correlation between VRP-derived velocity estimates and porosity-derived velocity estimates suggests that (1) our inversion method is capable of accurately determining EM velocity values, and (2) VRP velocity estimates may be used to estimate porosity or water content values in coarse alluvial sediments.

In general, the porosity-derived velocity estimates are a little slower than the VRP-derived velocity estimates. This discrepancy may be due to two factors. First, the neutron count-porosity conversion is based upon the empirical relation (Hearst and Nelson, 1985; Barrash and Clemo, 2002):

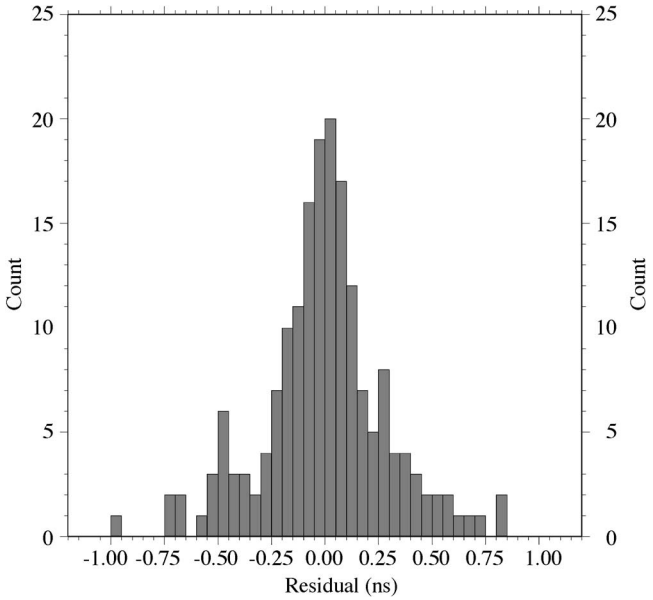

Figure 6. Histogram of traveltime residuals. The mean traveltime residual is 0.00 ns with a standard deviation of 0.30. The residuals range from −1.00 to 0.85 ns.

$$\phi = 10^{(N-A)/B}, \quad (14)$$

where N is the neutron tool reading (counts/second), A and B are the tool readings for two different known or estimated porosity values in the aquifer, and ϕ is the porosity. In Figure 5, the porosity-derived EM velocity estimates are based on assumed values for A and B, not the results of a physical calibration experiment using sediments of known porosity from the BHRS.

Second, systematic errors in the traveltime data may arise from errors in the time zero correction or the sampling frequency. These errors will also effect the relationship between radar velocity (or slowness) and porosity. However, testing shows that large traveltime delays have little effect on the inverted velocities below about 2-m depth.

Error analysis

A significant (although underutilized) advantage of an inversion method is that estimates of the reliability of the model parameters are provided. To further test the validity of our model, the inversion computed some statistical measures of the uncertainty in the re-

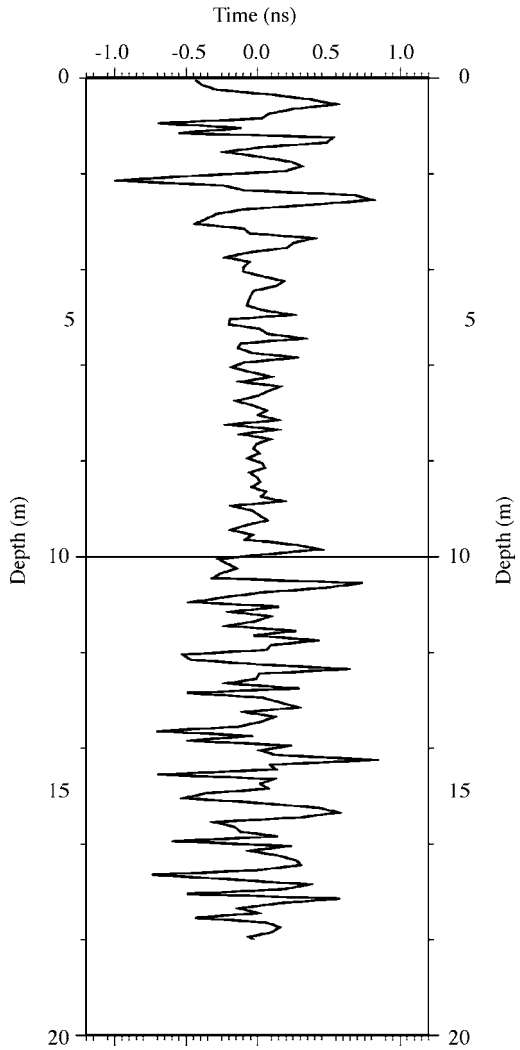

Figure 7. Traveltime residuals plotted versus depth. The magnitude of the residuals increases dramatically below 9.5-m depth.

sults. Figure 6 shows a histogram of the traveltime residuals. The residuals range from −1.00 to 0.85 ns, with a mean value of 0.00 ns, a standard deviation of 0.30 ns, and an rms value of 0.02 ns. The small value of the standard deviation indicates that the model predicts the data well.

The distribution of the residuals with depth can also help assess the uncertainty in the model (Figure 7). The large magnitude residuals at depths of about 1 and 2 m occur where reflections are observed in the VRP. The reflections imply large velocity contrasts. As mentioned, the inversion seeks a smooth velocity distribution. The coincidence of the large residuals with the reflections indicates that the velocity estimates are artifacts of the inversion algorithm. The large residuals at these depths emphasize the importance of understanding the assumptions in the inversion method.

At depths greater than 9.5 m, the magnitude of traveltime residuals increases significantly (Figure 7). The large residuals at depths greater than 9.5 m also correlate with the deeper, more uncertain traveltime picks. A careful examination of the picks plotted in Figure 4 show that at depths greater than 9.5 m, the picks do not form as smooth a line as they do at shallower depths. Also, at depths greater than 13 m, the noise in the data becomes more prominent. In our inversion, we assigned a single uncertainty to the observations. Figure 7 suggests that the uncertainty changes with depth. Clearly, knowledge of data uncertainty is critical for obtaining an accurate uncertainty analysis for the model.

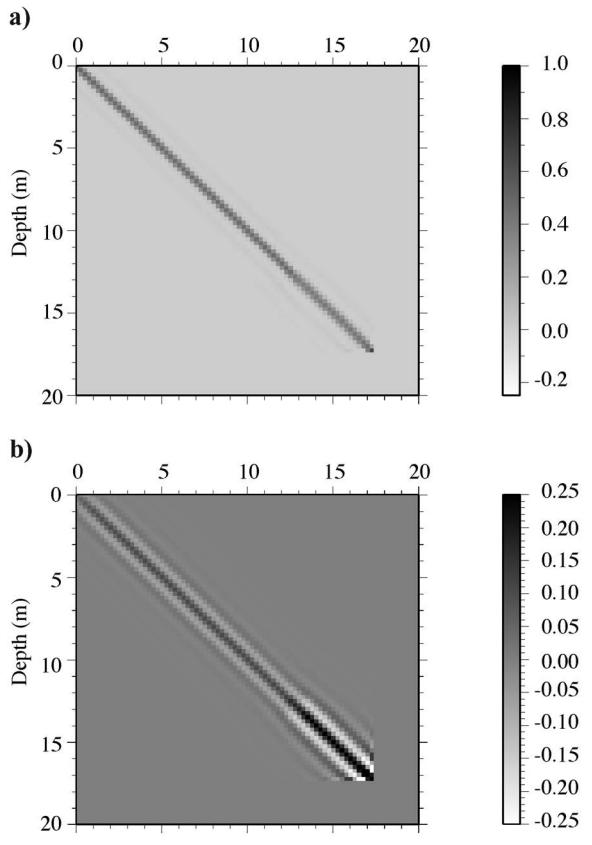

Figure 8. The complete model resolution and model covariance matrices showing the influence of the off-diagonal elements. (a) The model resolution matrix. (b) The model covariance matrix. In the covariance matrix plot, the scale is limited to emphasize the diagonal elements of the matrix. Values greater than 0.25 are black; values less than −0.25 are white.

Analysis of the model resolution (equation 8) and model covariance (equation 9) matrices provide further insight into the validity of the model. By computing the model resolution and model covariance matrices, we can note where the model parameters are well or poorly constrained. Figure 8 shows the model resolution and model covariance matrices for the velocity model. In our VRP inversion, the narrow strip along the diagonal of the model resolution matrix to a depth of about 13 m indicates that the velocity determined for each layer is based on the velocities from a few adjacent layers. Similarly, the narrow strip along the diagonal of the covariance matrix above depths of 13 m indicates that the uncertainty in velocity estimates depends only on a few adjacent layers. At depths greater than 13 m, model resolution values decrease and the width of the diagonal increases slightly. For the covariances, the magnitudes of the values increase as does the width of the diagonal. These trends indicate that the model is less certain at deeper depths, as expected.

To provide more detail, Figure 9 shows the diagonal elements from the model resolution and model covariance matrices. The velocities are best resolved near the surface, then the model resolution gradually decreases to about 0.43 near a depth of 3 m. Model resolution values of 0.43 indicate that the velocities are weighted only slightly by adjacent layer velocities. The diagonal elements of the covariance matrix (the variances) are low near the surface and increase to 0.10 ns^2/m^2 at a depth of about 3 m. In our model, the variance is nearly constant at depths between 3 m and about 13 m, indicating that the uncertainty in the velocities is about the same at these depths. At depths greater than 13 m, the model resolution decreases to 0.34, and the variance increases to 0.25 ns^2/m^2. From

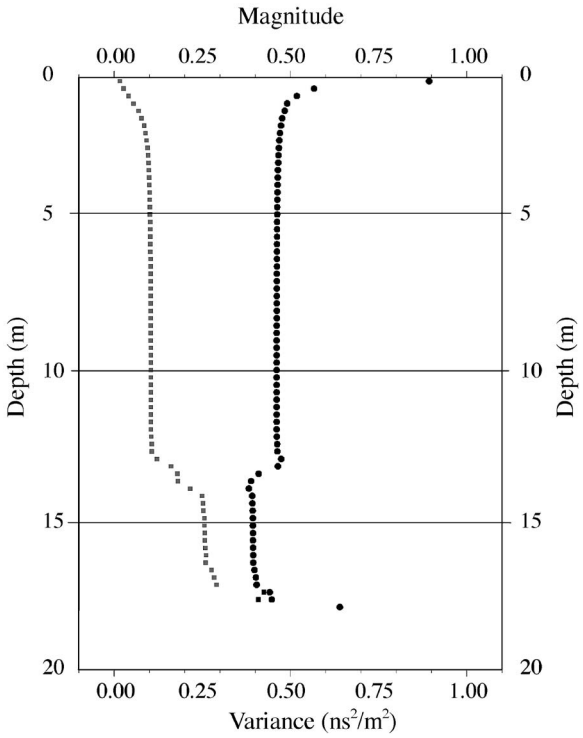

Figure 9. The diagonal of the model resolution (black circles) and the model covariance (gray squares) matrix of the inverted model shown in Figure 5. Each diagonal element of the covariance matrix is equal to the slowness variance of that parameter of the model.

computing the model resolution and model covariance matrices, we see that the model parameters at depths greater than 13 m are less certain than the shallower model parameters.

Our analysis of the model resolution and model covariance matrices relies on linear inverse theory. As mentioned earlier, the VRP problem is nonlinear. We have assumed that the radar energy propagates between the transmitter and the receiver in a straight path. In reality, the energy refracts at velocity changes according to Snell's law. Our appraisal analysis does not account for the error introduced by curved raypaths. The analysis also assumes the inversion has found the global minimum. At the minimum, the method uses linear theory to find the model resolution and model covariance matrices. However, if the solution is not at the global minimum, the velocity model is incorrect even though the model resolution and model covariance matrices indicate small errors in model parameters.

Another, more visual, method for analyzing reliability is shown in Figure 10. We used the information contained in the model covariance matrix to generate realizations of our model. Following Gouveia and Scales (1998), we take several steps to compute models that fit the data to within the model uncertainty. The first step is to compute the **LU** (lower and upper triangular) decomposition of the model covariance matrix. Next, we compute a normally distributed, pseudorandom number sequence with zero mean and unit variance. Finally, we take the inner product of the lower triangular (**L**) part of the **LU** decomposition and the pseudorandom numbers to get a single model realization. This realization has the same covariance as our model, and thus represents another possible model that fits within the uncertainty of our data. Figure 10a shows 80 such realizations. We have high confidence in those features that

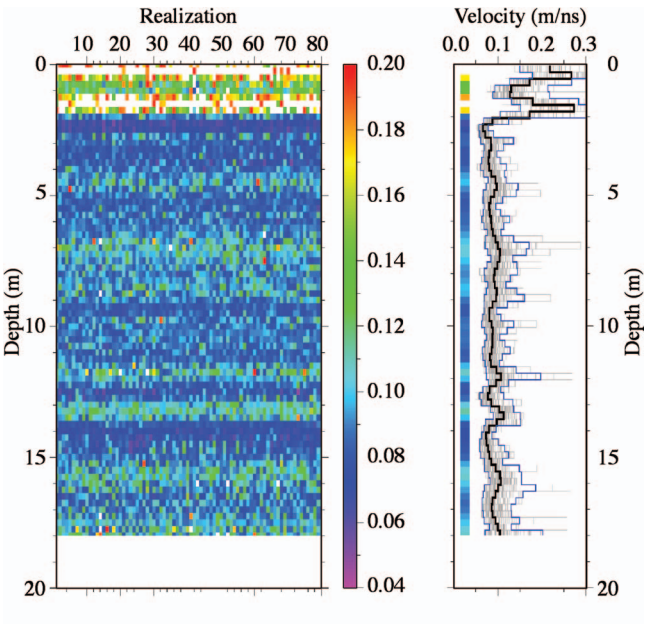

Figure 10. Plot of simulations with the same model covariance values as the inverted model. (a) Plot of 80 realizations of the statistically equivalent models. Horizontal lines in the plot indicate layer velocities that are well resolved by the inversion. (b) Plots the 80 models (gray lines) from the simulation along with the color-coded inverted velocity model. Our inverted model is superimposed as the black line. The 95% confidence bounds are also plotted as blue lines.

are laterally continuous. Figure 10b shows overlays of the velocity models from these 80 simulations, including the 95% confidence intervals based on twice the standard deviation of the model parameters. We computed the error bars based on the standard deviations derived from the 80 slowness model simulations:

$$\sigma = \sqrt{\frac{\sum_{i=1}^{N} (\mathbf{m_i} - \bar{\mathbf{m}})^2}{(N-1)}}, \tag{15}$$

where $\mathbf{m_i}$ is a particular slowness model parameter vector and $\bar{\mathbf{m}}$ is the average of the N = 80 realizations. The velocity-model parameters with error bounds then become

$$\frac{1}{\bar{\mathbf{m}} + 2\sigma} \leq \mathbf{v} \leq \frac{1}{\bar{\mathbf{m}} - 2\sigma}. \tag{16}$$

Figure 10 shows that the model is more reliable at depths greater than 2 m. Gouveia and Scales (1998) point out that error estimates based on the standard deviation ignore the contribution from the off-diagonal elements of the model covariance matrix. In many papers, the standard deviations are incorrectly computed as the square root of the diagonal elements of the covariance matrix. These standard deviations result in the error bounds marked with the red lines in Figure 5. This method does not account for the nonlinear relationship between slowness and velocity. Although these standard deviations tightly constrain the velocity model compared to the correct error bars, they falsely overconstrain the model. Figures 5 and 10 demonstrate the importance of incorporating the off-diagonal elements of the covariance matrix and recognizing the nonlinear aspect of the error estimation.

CONCLUSION

We used a linear, weighted, damped least-squares inversion algorithm to invert VRP traveltimes for a layered velocity model. This inversion algorithm computed the generalized inverse to estimate the model resolution and model covariance matrices. Using these matrices, we examine the uncertainty of our model. Thus, we can provide estimates about the reliability of our results, an important consideration in decision making.

The synthetic study indicates that the straight-ray approximation is valid for depths greater than about 2 m in our experiment. The inversion procedure worked well for the noise-free traveltimes; the inverted model parameters matched the input model for depths greater than 2.0 m. We added noise to the traveltimes to investigate the inversion method's capability with more realistic data. To reasonably match the input model, we had to regularize the inversion. The smoothness constraint and the noise caused small fluctuations in the model parameters, but the large-scale velocity changes are still apparent in the inverted model.

We inverted VRP data acquired at a sand-and-gravel, unconfined aquifer. Our model consists of velocities ranging between 0.12 and 0.27 m/ns for the shallowest 2 m, and between 0.06 m/ns to 0.1 m/ns for depths greater than 2 m. The high velocities probably indicate that the first arrivals near the surface consist of refracted waves. Otherwise, the velocities correspond well with changes in porosity and changes in the geology beneath the site. The modeled velocity magnitudes are in approximate agreement

with velocities derived from neutron logs, providing an independent corroboration of our model.

The model is best constrained at depths between 2 and 10 m, based on the size of the traveltime residuals, the model resolution and model covariance analysis, and our model realization method. The shallowest 2 m of the model are the most uncertain; the straight-raypath assumption is clearly violated by refracted air waves along the surface. However, the straight-ray assumption is necessary to linearize the inverse problem. The large uncertainty for depths greater than 13 m may be because of a decreased signal to noise ratio. Interestingly, the formal model resolution and model covariance analyses indicate the model is best constrained near the surface. Between depths of 3 and 13 m, the model resolution and model covariance values are constant. The difference in uncertainty between the formal analysis and the model-realization method underscores the importance of the off-diagonal elements of the covariance matrix.

VRP velocity models provide insight into the distribution of physical properties, such as porosity, in the subsurface. These velocities can be used as starting models for tomography studies or as velocity information for surface reflection processing steps, such as migration and time-to-depth conversion at the same site. The velocity information gained from VRPs provide valuable information for characterizing the shallow subsurface.

ACKNOWLEDGMENTS

The U. S. Army Research Office grants DAAH04-96-1-0318, DAAG55-98-1-0277, and DAAD19-00-1-0454 funded this project. Undergraduate students E. Badeau (New England College) and Ann Erickson (Reed College) helped acquire the vertical radar profile field data at the Boise Hydrogeophysical Research Site. NSF REU project EEC-9820448 supported Eric Badeau. We acknowledge support of this research by Landmark Graphics Corporation via the Landmark University Grant Program. We gratefully acknowledge cooperative agreements with the Idaho Transportation Department, the U. S. Bureau of Reclamation, and Ada County for the development and use of the BHRS site. This work is contribution no. 0118 of the Center for Geophysical Investigation of the Shallow Subsurface at Boise State University.

REFERENCES

Aki, K., and P. G. Richards, 1980, Quantitative seismology: Theory and practice: W. H. Freeman.

Barrash, W., and T. Clemo, 2002, Hierarchical geostatistics and multifacies systems: Boise Hydrogeophysical Research Site: Boise, Idaho: Water Resources Research, **38**, 1196, doi:10.1029/2002/WR001436.

Barrash, W., and M. D. Knoll, 1998, Design of research wellfield for calibrating geophysical methods against hydrologic parameters: Proceedings of the 13th Annual Conference on Hazardous Waste Research, 296–318.

Binley, A., P. Winship, R. Middleton, M. Pokar, and J. West, 2001, High-resolution characterization of vadose zone dynamics using cross-borehole radar: Water Resources Research, **37**, 2639–2652.

Buursink, M. L., J. W. Lane, W. P. Clement, and M. D. Knoll, 2002, Use of vertical-radar profiling at two New England sites and comparison with neutron log porosity: Presented at the 15th Annual Symposium on the Application of Geophysics to Engineering and Environmental Problems, Environmental and Engineering Geophysical Society, 12.

Cassini, G., C. Strobbia, and L. Gallotti, 2004, Vertical radar profiles for the characterization of the deep vadose zone: Vadose Zone Journal, 3, 1093–1105.

Constable, S. C., R. L. Parker, and C. Constable, 1987, Occam's inversion: A practical algorithm for generation of smooth models from electromagnetic sounding data: Geophysics, **52**, 289–300.

Davis, J. L., and A. P. Annan, 1989, Ground-penetrating radar for high-resolution mapping of soil and rock stratigraphy: Geophysical Prospecting, **37**, 531–551.

Gouveia, W., and J. A. Scales, 1998, Bayesian seismic waveform inversion: Parameter estimation and uncertainty analysis: Journal of Geophysical Research, **103**, 2759–2779.

Greaves, R. J., D. P. Lesmes, J. M. Lee, and M. N. Toksöz, 1996, Velocity variations and water content estimated from multi-offset, ground-penetrating radar: Geophysics, **61**, 683–695.

Hearst, J. R., and P. H. Nelson, 1985, Well logging for physical properties: McGraw-Hill.

Hole, J. A., and B. C. Zelt, 1995, 3-D finite-difference reflection traveltimes: Geophysical Journal International, **121**, 427–434.

Knoll, M. D., 1996, A petrophysical basis for ground penetrating radar and very early time electromagnetics: Electrical properties of sand-clay mixtures: Ph.D. thesis, University of British Columbia.

Knoll, M. D., and W. P. Clement, 1999, Vertical radar profiling to determine dielectric constant, water content and porosity values at well locations: Presented at the 11th Annual Symposium on the Application of Geophysics to Engineering and Environmental Problems, Environmental and Engineering Geophysical Society, 821–830.

Knoll, M. D., and R. J. Knight, 1994, Relationships between dielectric and hydrogeologic properties of sand-clay mixtures. Proceedings of the Fifth International Conference on Ground Penetrating Radar, The Ohio State University, 45–61.

Lines, R. L., A. Bourgeois, and J. D. Covey, 1984, Traveltime inversion of offset vertical seismic profiles — A feasibility study: Geophysics, **49**, 250–264.

Lizarralde, D., and S. Swift, 1999, Smooth inversion of VSP traveltime data: Geophysics, **64**, 659–661.

Menke, W., 1989, Geophysical data analysis: Discrete inverse theory: Academic Press, Inc.

Moret, G. J. M., W. P. Clement, M. D. Knoll, and W. Barrash, 2004, VSP traveltime inversion: Near-surface issues: Geophysics, **69**, 345–351.

Parker, R. L., 1994, Geophysical inverse theory: Princeton University Press.

Peterson, J. E. Jr., E. L. Majer, and M. D. Knoll, 1999, Hydrogeological property estimation using tomographic data at the Boise Hydrogeophysical Research Site: Presented at the 12th Annual Symposium on the Application of Geophysics to Engineering and Environmental Problems, Environmental & Engineering Geophysical Society, 629–638.

Pringle, J. K., A. R. Westerman, J. D. Clark, J. A. Guest, R. J. Ferguson, and A. R. Gardiner, 2003, The use of vertical radar profiling (VRP) in GPR surveys of ancient sedimentary strata, C. S. Bristow and H. M. Jol, eds., Ground penetrating radar in sediments: Geological Society of London, Special Publications **211**, 225–246.

Pujol, J., R. Burridge, and S. B. Smithson, 1985, Velocity determination from offset vertical seismic profiling data: Journal of Geophysical Research, **90**, 1871–1880.

———, 1986, Velocity determination from offset VSP data: Tests of the method: Journal of Geophysical Research, **91**, 701–708.

Snieder, R., and J. Trampert, 1999, Inverse problems in geophysics: Samizdat Press.

Stewart, R. R., 1984, Vertical-seismic-profile (VSP) interval velocities from traveltime inversion: Geophysical Prospecting, **32**, 608–628.

Tillard, S., and J.-C. Dubois, 1995, Analysis of GPR data: Wave propagation velocity determination: Journal of Applied Geophysics, **33**, 77–91.

Tronicke, J., K. Holliger, W. Barrash, and M. D. Knoll, 2004, Multivariate analysis of cross-hole georadar velocity and attenuation tomograms for aquifer zonation: Water Resources Research, **40**, W01519, doi:10.1029/2003WR002031.

Tronicke, J., and M. D. Knoll, 2005, Vertical radar profiling: Influence of survey geometry on first arrival traveltimes and amplitudes: Journal of Applied Geophysics, **57**, 179–191.

van Wijk, K., J. A. Scales, W. Navidi, and L. Tenorio, 2002, Data and model uncertainty estimation for linear inversion: Geophysical Journal International, **149**, 625–632.

Wharton, R. P., G. A. Hazen, R. N. Roy, and D. L. Best, 1980, Electromagnetic propagation logging: Advances in technique and interpretation: SPE, Paper 9267.

Zhou, H., and M. Sato, 2000, Application of vertical radar profiling technique to Sendai Castle: Geophysics, **65**, 533–539.